

# Modelling Mg<sub>2</sub>Si Dissolution in an AA6063 Alloy During Pre-heating to the Extrusion Temperature

J. van de Langkruis<sup>1</sup>, N. C. W. Kuijpers<sup>2</sup>, W. H. Kool<sup>1</sup>, F. J. Vermolen<sup>3</sup>, S. van der Zwaag<sup>1,2</sup>  
<sup>1</sup>Lab. for Materials Science, Delft University of Technology, Delft, The Netherlands,  
<sup>2</sup>Netherlands Institute for Metals Research, Delft, The Netherlands, <sup>3</sup>CWI, Amsterdam, The Netherlands.

---

## ABSTRACT

A finite volume model was used to calculate Mg<sub>2</sub>Si particle dissolution and the solute Mg content in an AA6063 extrusion alloy during pre-heating to the extrusion temperature. The model contains a limited number of physical parameters, which are obtained from the literature. Firstly, the model was validated with DSC experiments. Secondly, dissolution diagrams were constructed, which show a strong dependence of solute Mg concentration after pre-heating on heating rate and initial Mg<sub>2</sub>Si particle size. The solute content can be used to predict the peak hardness after artificial ageing. When the initial Mg<sub>2</sub>Si particle size and volume fraction are known, the dissolution diagrams can be used to determine the maximum allowable pre-heating rate before extrusion leading to a maximum peak hardness in the final product.

---

## INTRODUCTION

Quantitative information concerning the presence or absence of Mg<sub>2</sub>Si precipitates and the Mg and Si solute content in an extrusion billet is valuable for assessing extrusion behaviour and peak hardness of the extrudate as a function of prior thermal history and composition. In the past, Mg<sub>2</sub>Si dissolution during pre-heating to extrusion temperatures has been modelled with classical phenomenological phase transformation theory [1-5]. However, this approach always incorporates numerous fitting parameters, which have to be optimised depending on the alloy and its thermal history. Also, some important effects, such as the contact surface between particles and aluminium matrix, and the saturation of the matrix at the particle interface, both affecting the reaction rate, cannot be calculated directly with this approach.

In recent years physical methods have been developed [6-8], which are capable of modelling particle dissolution and growth in binary and more complex systems. These models do not need fitting parameters, but depend on physical parameters, such as solubility products and diffusion coefficients for the alloying elements in the matrix.

Vermolen *et al.* [8] developed a finite volume model for dissolution of a multi-component particle, and calculated the dissolution of Mg<sub>2</sub>Si-precipitates in an industrial AlMgSi alloy. Vermolen's finite volume model was applied to estimate the solute content after pre-heating in a Mg<sub>2</sub>Si-containing AA6063 alloy, and to correlate the Mg and Si solute content to the

hot flow stress and the peak hardness after artificial ageing [9].

In the present paper the finite volume model was validated experimentally by calculating and measuring Mg<sub>2</sub>Si dissolution during Differential Scanning Calorimetry (DSC) experiments. DSC experiments are very suitable for studying particle dissolution in metals, as the heat flow is directly proportional to the dissolution rate. Furthermore, the model was used to construct a diagram of the Mg solute content after pre-heating as a function of the initial Mg<sub>2</sub>Si particle radius and the heating rate. The diagram can be used to predict the obtainable peak hardness.

## THE PARTICLE DISSOLUTION MODEL

The model [8] considers the dissolution process of a spherical Mg<sub>2</sub>Si particle of initial radius  $r=r_0$ , surrounded by an aluminium matrix cell with cut-off radius  $r=R_{Al}$ , as depicted in Figure 1. The Al cell size  $R$  is chosen such that  $(r_0^3/R_{Al}^3)$  is equal to the volume fraction of the Mg<sub>2</sub>Si particles in the alloy.

During pre-heating the temperature  $T(t)$  increases from room temperature to the extrusion temperature. As a result of dissolution, the particle radius,  $r_p(t)$ , will decrease with time which is calculated by the model ( $r_p(0)=r_0$ ).

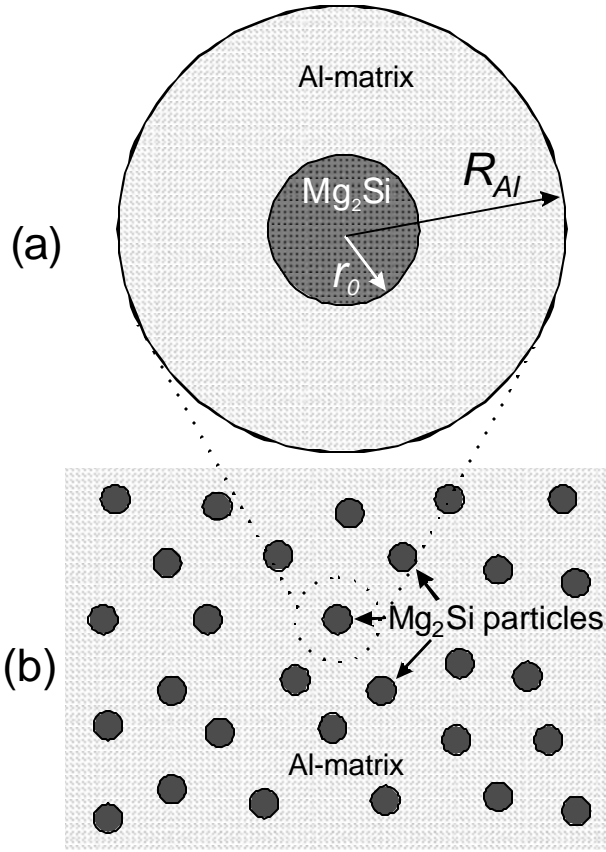


Figure 1 (a) Modelled configuration, indicating  $r_0$  and  $R_{Al}$ . (b) Schematic display of the microstructure of the aluminium alloy with  $Mg_2Si$  precipitates.

It is assumed that at the start of the preheating process ( $t=0$ ) the initial Mg- and Si- concentrations in the matrix are uniform with  $c_{Mg}^{init}$  and  $c_{Si}^{init}$  (wt%). The diffusive flux of Mg or Si in the matrix is taken to be independent of the presence of Si or Mg in the matrix, respectively. For the concentrations of both elements ( $c_{Mg}$  and  $c_{Si}$ ) the diffusion may be represented by Fick's second law in spherical co-ordinates:

$$\frac{\partial c_i}{\partial t} = \frac{D_i}{r^2} \frac{\partial}{\partial r} \left( r^2 \frac{\partial c_i}{\partial r} \right) \quad (1)$$

where  $i=Mg, Si$ .

For each element Mg and Si the diffusion coefficient  $D_i$  in the aluminium matrix is given by an Arrhenius relationship:

$$D_i = D_i^0 \exp \left( -\frac{Q_i^d}{RT(t)} \right) \quad (2)$$

where  $R$  is the molar gas constant. The diffusion parameters  $D_i^0$  and  $Q_i^d$  have been determined

experimentally by Fujikawa [10], and are listed in Table 1.

In the model three boundary conditions are imposed. The first one is for the concentrations in the Al-matrix on the interface of the precipitate, where for both the Mg and Si concentrations the Dirichlet boundary condition is used:

$$(c_i)_{r=r_p} = c_i^{sol} \quad (3)$$

The concentrations  $c_{Mg}^{sol}$  and  $c_{Si}^{sol}$  are not constant, but change in time. Assuming local equilibrium at the interface of the precipitate, these concentrations are connected by the following hyperbolic relation [8]:

$$(c_{Si}^{sol})^{1/3} \cdot (c_{Mg}^{sol})^{2/3} = K_0 \exp \left( \frac{-Q_{sol}}{RT(t)} \right) \quad (4)$$

where the powers of the concentrations on the left hand side of the equation correspond to the stoichiometric  $Mg_2Si$ -phase. The right hand side of eq. (4) is the solubility product, where  $K_0$  is a pre-exponential factor, and  $Q_{sol}$  is the activation energy for the solubility. The solubility parameters are taken from literature [11] and are given in Table 1.

The second boundary condition applies to the matrix-boundary at  $r=R_{Al}$  where there is no flux through the boundary, for both Mg and Si concentrations:

$$\left( \frac{\partial c_i}{\partial r} \right)_{r=R_{Al}} = 0 \quad (5)$$

The third boundary condition arises when the  $Mg_2Si$  particle is completely dissolved. In that case, from symmetry considerations there can be no flux through the centre of the Al cell, and therefore, for both Mg and Si concentrations a new Neumann boundary condition must be imposed:

$$\left( \frac{\partial c_i}{\partial r} \right)_{r=0} = 0 \quad (6)$$

In the model it is assumed that the composition of the  $Mg_2Si$  precipitates remains stoichiometric at all times, and that there is no volume change of the cell when the  $Mg_2Si$ -particle dissolves in the Al-matrix. Therefore the density of  $Mg_2Si$  is taken equal to that of the aluminium matrix.

From conservation of mass and the stoichiometry of the  $Mg_2Si$  particle, the interfacial particle-matrix velocity can be derived from the interfacial gradients of the Mg- or the Si-concentration in the Al-matrix:

$$\begin{aligned} \frac{dr_p(t)}{dt} &= \frac{D_{Mg}}{c_{Mg}^p - c_{Mg}^{sol}(t)} \left( \frac{\partial c_{Mg}}{\partial r} \right)_{r=r_0} \\ &= \frac{D_{Si}}{c_{Si}^p - c_{Si}^{sol}(t)} \left( \frac{\partial c_{Si}}{\partial r} \right)_{r=r_0} \end{aligned} \quad (7)$$

where  $c_{Mg}^p$  and  $c_{Si}^p$  are the stoichiometric concentrations of the particle.

Table 1 Diffusion and solubility parameters with literature source.

Parameter	Value	
$D_{Mg}^0$	$0.49 \cdot 10^{-4} \text{ m}^2/\text{s}$	[10]
$Q_{Mg}^d$	124 kJ/mol	[10]
$D_{Si}^0$	$2.02 \cdot 10^{-4} \text{ m}^2/\text{s}$	[10]
$Q_{Si}^d$	136 kJ/mol	[10]
$K_0$	89 wt%	[11]
$Q_{sol}$	31.97 kJ/mol	[11]

## EXPERIMENTAL DETAILS

An AA6063 billet with a composition given in Table 2, was industrially extruded to a rectangular profile with dimensions  $1000 \times 100 \times 30 \text{ mm}^3$ . SEM specimens were taken from the central part, and homogenised at 853 K (580 °C) for 6 hours in an air furnace and subsequently down-quenched in a salt bath to 640 K (367 °C), pre-aged for 13.3 hours to induce precipitation of  $\beta \text{ Mg}_2\text{Si}$  particles, and then water quenched. This material condition is designated as *b-fine*.

Table 2 Alloy composition in wt%.

Mg	Si	Fe	Cu, Mn, Cr, Zr, Pb	Ti
0.45	0.40	0.19	<0.01	0.01

From SEM images the effective  $\text{Mg}_2\text{Si}$  particle radius,  $r_0$ , for this material condition, was estimated. The initial solute concentrations after pre-ageing ( $c_{Mg}^{init}$  and  $c_{Si}^{init}$ ) and the  $\text{Mg}_2\text{Si}$  volume fraction were calculated with the software package MTDATA [12]. With these values and using mass conservation, the Al-cell radius,  $R$ , was calculated for the *b-fine* condition. These parameters of the  $\beta$ -fine condition are given in Table 3.

Table 3 Parameters values for *b-fine*.

parameter	value
$r_0$	$0.40 \pm 0.2 \text{ } \mu\text{m}$
$\text{Mg}_2\text{Si}$ volume fraction	0.65 vol%
$R$	$2.14 \pm 0.5 \text{ } \mu\text{m}$
$c_{Mg}^{init}$	0.067 wt%
$c_{Si}^{init}$	0.19 wt%

For the DSC experiments, disc-shaped polished samples with a diameter of  $\varnothing 5 \text{ mm}$  and a thickness of about 0.6 mm were obtained from the centre of the extrusion profile. DSC experiments were carried out, using a Perkin & Elmer DSC 7. The DSC-samples were treated *in situ* in the DSC equipment with the same temperature scheme as used for the SEM specimens [9, 13]. Scans are taken from 273 K (0 °C) to 853 K (580 °C) with heating rates of 10 or 170 K/min.

The experimental heat flow (J/K) measured by DSC is directly compared to the dissolution rate of the particle (vol%/K), as calculated by the finite volume model, using the data in Table 3.

Further, the solute Mg content after preheating was calculated. The pre-heating process, used in these calculations consists of linear heating (with a heating rate  $dT/dt$ ) to 773 K and holding at the same temperature for a certain time. For the calculations the initial matrix concentrations and  $\text{Mg}_2\text{Si}$  volume fraction of  $\beta$ -fine are used (Table 3), where the heating rate ( $dT/dt$ ), initial partial radius ( $r_0$ ) and holding time are varied. As a result, examples of dissolution diagrams are constructed which depict the calculated solute Mg content after preheating as a function of heating rate and initial particle radius  $r_0$ . The Mg solute content in the dissolution diagrams is calculated by averaging the Mg concentration ( $c_{Mg}(r)$ ) in the matrix.

## RESULTS

### Heat Effects Due to $\text{Mg}_2\text{Si}$ Dissolution

In Figure 2 the modelled dissolving volume per Kelvin and the measured DSC heat flow for the *b-fine* condition are given. It can be observed that in the experimental 10 K/min curve the onset-, peak- and end temperatures are lower than the corresponding temperatures of the experimental 170 K/min curve, which is a result of kinetic effects. The peak positions of the experimental curves are predicted well by the numerical calculations. In contrast to the experimental curves, where the dissolution speed displays a tail at higher temperature, the calculated curves show a

sharp decrease in dissolution speed. Chen *et al.* [14] showed that this tail can be explained by incorporating a complete particle distribution. However, taking one effective particle radius instead of the complete distribution does not significantly affect the calculated peak positions.

To assess the sensitivity of the model to the value taken for the initial particle radius, a calculated 170 K/min-curve for  $r_0 = 0.22 \mu\text{m}$ , with the same particle volume fraction as *b-fine*, is also added in Figure 2. It can be observed that there is a significant shift of the dissolution peak to lower temperatures, indicating that the results of the calculations are largely influenced by the particle size.

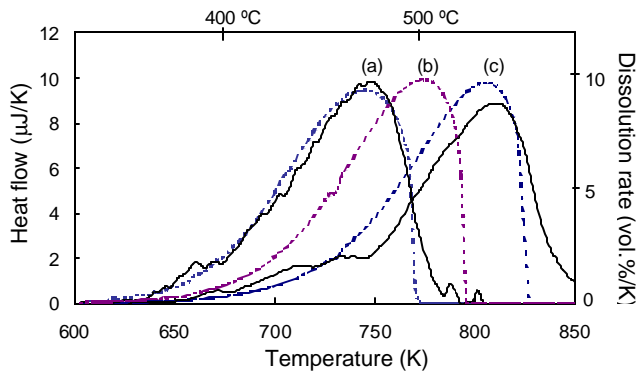


Figure 2 Experimental DSC curve (solid line) and calculated dissolution rate (dashed line). (a)  $dT/dt = 10 \text{ K/min}$ ,  $r_0 = 0.40 \mu\text{m}$  (b)  $dT/dt = 170 \text{ K/min}$ ,  $r_0 = 0.22 \mu\text{m}$ . (c)  $dT/dt = 170 \text{ K/min}$ ,  $r_0 = 0.40 \mu\text{m}$ .

### The Effect of Initial Particle Size and Heating Rate

Having established the satisfying accuracy of the model for some specific cases it can now be used to predict the effect of initial  $\text{Mg}_2\text{Si}$  particle size and heating rate upon the final solute content at the end of a pre-heating procedure.

In Figure 3 Mg dissolution diagrams are given, constructed for two holding times: (a) 4s; (b) 5 minutes. The dissolution diagrams show the iso-solute Mg contours. The numbers in the figure indicate the Mg solute content (wt%). The shaded areas represent the conditions for which the particles are completely dissolved after preheating, and the solute content is at its maximum. The diagrams indicate that the solute content after pre-heating decreases with increasing initial particle size and increasing heating rate. Furthermore, it can be observed that the final solute Mg content is significantly influenced by the holding time.

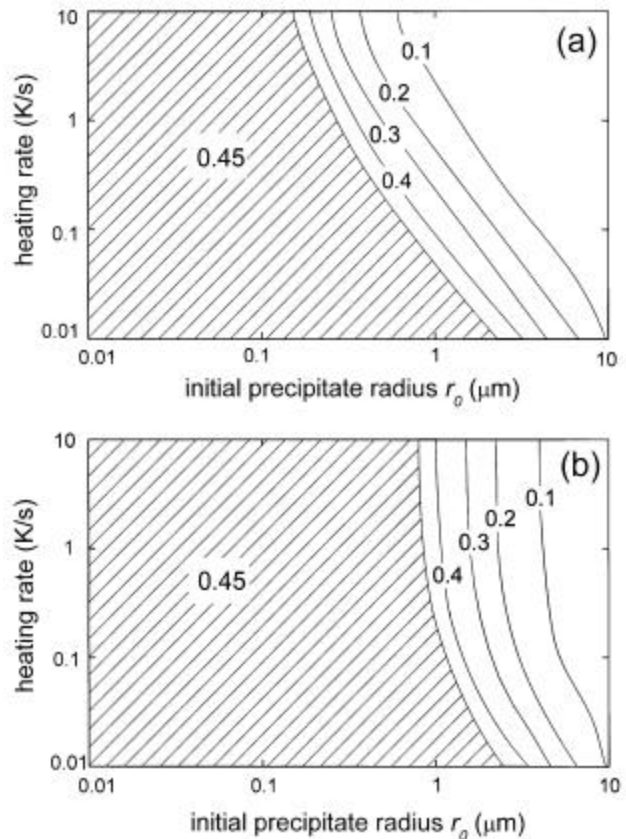


Figure 3 Mg solute content after pre-heating, as a function of heating rate and initial particle radius (a) holding time 4 s; (b) holding time 5 minutes.

### DISCUSSION

The comparison of DSC experiments and numerical calculations shows good agreement over a wide range of heating rates, even when using standard literature values for the physical parameters. Under conditions of high heating rates and relatively small particles ( $< 0.5 \mu\text{m}$ ) the results of the calculations are very sensitive to the value of the initial particle diameter.

The dissolution diagrams show that for longer holding times and heating rates  $\geq 0.3 \text{ K/s}$  the heating rate does not strongly influence the final solute Mg content, because most of the dissolution takes place during holding.

To illustrate how the model can be used to predict obtainable mechanical properties, a simple method to estimate the peak hardness after a standard peak ageing treatment in an AA6063 alloy is described, following the approach of Bratland *et al.* [2]. For excess Si alloys, the peak hardness,  $H_{\text{sample}}$ , after a given artificial ageing treatment, is related to its solute Mg content,  $c_{\text{Mg,matrix}}$ , after pre-heating, but before

ageing, as well as to the maximum peak hardness increase obtainable with the given ageing treatment, through

$$H_{sample} = H_{over} + \frac{C_{Mg,matrix}}{C_{Mg,alloy}} \times \Delta H. \quad (8)$$

Here  $\Delta H$  is the hardness difference between a peak hardened fully solutionised sample and an extensively over-aged sample  $H_{over}$ , and  $C_{Mg,alloy}$  is the nominal Mg alloy content. When using eq. (8) it is assumed that the increase during peak ageing can be attributed completely to the formation of  $\beta''$ , and that all other effects on the hardness, such as the effect of dislocations and the effect of solute Si, are incorporated in  $H_{over}$  or do not influence the peak ageing behaviour significantly. In previous work [9] it was found that for the same alloy as in this work,  $\Delta H = 41$  HV and  $H_{over} = 39$  HV. The nominal composition  $C_{Mg,alloy} = 0.45$  wt%. The finite volume model calculates a value of  $C_{Mg,matrix} = 0.3$  wt% (see Figure 3a) for the *b-fine* condition after heating up with 170 K/min (2.83 K/s) and holding for 4s.  $H_{sample}$  is predicted 66 HV, close to the measured value of 70 HV, found previously [9], which demonstrates the applicability of dissolution diagrams as given in Figure 3.

Such dissolution diagrams can be used to determine under which conditions the particles dissolve completely and maximum peak hardness can be expected. Also, the solute dependency of the hot flow stress can be modelled [15-16]. Depending on the required mechanical properties the combinations of heating rate and initial particle diameters can be optimised. For instance, for a minimal peak hardness of 70 HV we derive from eq. (8) that the necessary Mg solute content before peak ageing is approximately 0.3 wt%, and then the diagram shows that with a typical industrial pre-heating rate of 20 K/min, the maximum allowable initial  $Mg_2Si$  particle size is 1  $\mu m$ .

Similar diagrams can be constructed, with iso-contours for the final particle radii after pre-heating. It is known [17] that large  $Mg_2Si$  precipitates can induce so-called incipient melting at the surface during extrusion. Assuming that incipient melting may occur for particles larger than a specific critical size, a critical range of initial radii and heating rates can be determined to prevent incipient melting of  $Mg_2Si$  at the extrudate surface.

Further research on the correlation between extrusion and extrudate behaviour and solute content is in progress.

## CONCLUSIONS

The dissolution behaviour of  $Mg_2Si$  precipitates of varying sizes in an AA6063 alloy was calculated with a finite volume model for varying particle diameters and heating rates. Some calculations were validated with DSC experiments and the agreement between calculations and experiments was satisfactory.

It was illustrated how the dissolution diagrams, calculated with the model, can be applied to predict the peak hardness, for a standard artificial ageing treatment, as a function of initial structure and pre-heating schedule to the extrusion temperature.

## ACKNOWLEDGEMENTS

This research is partially supported by the Technology Foundation (STW). We thank Boal Profielen BV for supplying the material, and Mr. S. P. Chen for valuable discussions, and Mr. C. G. Borsboom and Mr. N. Geerlofs for technical support.

## REFERENCES

1. D. A. Porter, K. E. Easterling, *Phase Transformations in Metals and Alloys*, second edition, Chapman & Hall, London, 1993.
2. D. H. Bratland, Ø. Grong, H. Shercliff, O. R. Myhr, S. Tjøtta, *Acta Mater.*, Vol. 45 1 (1997) 1.
3. J. D. Bryant, *Proc. Conf. on Automotive Alloys*, Orlando, Florida, Eds. S. K. Das, G. J. Kipouros, The Minerals, Metals, & Materials Society, Warrendale, 1997, p. 19.
4. S. P. Chen, K. M. Mussert, S. van der Zwaag, *J. Mat. Sci.* 33 (1998) 4477.
5. R. T. Shuey, J. P. Suni, R. D. Doherty, D. J. Chakrabarti, *Mat. Sci. Forum* Vols. 217-222 (1996) 735.
6. U. H. Tundal, N. Ryum, *Met. Trans.* 23A (1992) 443.
7. F. J. Vermolen, H. M. Slabbekoorn, S. van der Zwaag, *Mat. Sci. Eng.* A231 (1997) 80.
8. F. J. Vermolen, K. Vuik, S. van der Zwaag, *Mat. Sci. Eng.* A254 (1998) 13.
9. J. van de Langkruis, W.H. Kool, C. M. Sellars, M. R. van der Winden, S. van der Zwaag, *Mat. Sci. Eng. A*, submitted.
10. S.-I. Fujikawa, *Defect and Diffusion Forum*, Vols. 143-147 (1997) 403.
11. Ø. Grong, *Metallurgical Modelling of Welding*, Institute of Materials, London, 1994.
12. R. H. Davies, A. T. Dinsdale, J. A. Gisby, S. M. Hodson, R. G. J. Ball, in *Proc. Conf. on:*

*Applications of Thermodynamics in the Synthesis and Processing of Materials*, Rosemont, The Minerals, Metals & Materials Society/AIME, Warrendale, 1995, 371.

13. J. van de Langkruis, M.S. Vossenbergh, To be published in *Proc. TMS 1999 Annual Meeting, Light Metals, Automotive Book*, San Diego, 1999.
14. S. P. Chen, M. S. Vossenbergh, F. J. Vermolen, J. van de Langkruis, S. van der Zwaag, *J. Mat. Sci.* (1999), in press.
15. J. van de Langkruis, W.H. Kool, S. van der Zwaag, *Mat. Sci. Eng. A266* (1999) 135.
16. A. Espedal, H. Gjestland, N. Ryum, *J. Scand. Met.* 18 (1989) 131.
17. O. Reiso, Ph. D. Thesis, Norwegian Institute of Technology, Trondheim, Norway, 1992.